VLTI/Hi-5: detection yield predictions for young giant exoplanets

C. Dandumont, R. Laugier, A. Emsenhuber, J. Gagne, O. Absil, et al.

C. Dandumont, R. Laugier, A. Emsenhuber, J. Gagne, O. Absil, A. Bigioli, M. Bonavita, G. Garreau, M. Ireland, M.-A. Martinod, J. Loicq, D. Defrère, "VLTI/Hi-5: detection yield predictions for young giant exoplanets," Proc. SPIE 12183, Optical and Infrared Interferometry and Imaging VIII, 1218327 (26 August 2022); doi: 10.1117/12.2627942

SPIE.

Event: SPIE Astronomical Telescopes + Instrumentation, 2022, Montréal, Québec, Canada

VLTI/Hi-5: detection yield predictions for young giant exoplanets

C. Dandumont[a,e], R. Laugier[b], A. Emsenhuber[c], J. Gagne[d], O. Absil[e], A. Bigioli[b], M. Bonavita[f], G. Garreau[b], M. Ireland[d], M.-A. Martinod[b], J. Loicq[e, h], and D. Defrre[b]

[a]Centre Spatial de Lige, Universit de Lige, Avenue Pr-Aily, 4031 Angleur, Belgium
[b]Institute of Astronomy, KU Leuven, 200D Celestijnenlaan, Leuven, Belgium
[c]Ludwig-Maximilians-Universitt Mnchen, Germany
[d]Universit de Montral, Canada
[e]ULiege, Belgium
[f]The Open University, United Kingdom
[g]The Australian National University, Australia
[h]Delft University of Technology, Netherlands

ABSTRACT

The Hi-5 instrument, a proposed high-contrast L' band (3.5-4.0 µm) nulling interferometer for the visitor focus of the Very Large Telescope Interferometer (VLTI), will characterize young extra-solar planetary systems and exozodiacal dust around nearby main-sequence stars. Thanks to VLTI's angular resolution ($\lambda/B = 5$ mas for the longest UT baseline), it will fill the gap between young giant exoplanets discovered by ongoing single-aperture direct imaging surveys and exoplanet populations discovered by radial velocity surveys.

In this paper, we investigate the exoplanet detection yield of Hi-5. First, we present the latest catalog of stars identified as members of young stellar associations within 150 pc of the Sun thanks to the BANYAN algorithm and other searches for young moving group members. Realistic exoplanet populations are then generated around these stars and processed with the SCIFYsim tool, the end-to-end simulator for the Hi-5 instrument. Then, two formation models are used to estimate the giant planet's luminosity. The first is the New Generation Planetary Population Synthesis (NGPPS), also known as the *Bern* model, and the second is a statistical model based on gravitational instability (hot-start model - AMES-Dusty model).

We show that Hi-5 is insensitive to cold-start planets but can detect giant hot-start planets. With ATs, more than 40 planets could be detected assuming 20 nights of observations. With its unique capabilities, Hi-5 is also able to constrain in mass the observed systems. Hi-5 is sensitive to planets with a mass $> 2\ M_{\rm jup}$ around the snow line.

Keywords: interferometry, exoplanets, astronomy, nulling, astronomy

1. INTRODUCTION

The first exoplanet around a Solar-like star was discovered 26 years ago[1] and since then more than 5000 exoplanets have been detected from the ground or space, but only a few directly.* Thanks to METIS/ELT[2] and new instruments for current facilities (GRAVITY+ and the ASGARD suite for the VLTI), high contrast imaging will be able to characterize a growing number of exoplanets and ultimately, with space-based projects like LIFE,[3] will spectrally characterize rocky planets.

We present here Hi-5, a high-contrast L'-band (3.5-4.0 µm) nulling interferometric instrument. The gain in contrast (10^{-5}) and spatial resolution will allow to directly detect giant exoplanets.[4] It will better constrain the evolutionary model of these exoplanets (cold or hot-start) and their distribution.

Further author information: Colin Dandumont, colin.dandumont@uliege.be
*As of July 13, 2022: https://exoplanets.nasa.gov/

Optical and Infrared Interferometry and Imaging VIII, edited by Antoine Mérand, Stephanie Sallum, Joel Sanchez-Bermudez,
Proc. of SPIE Vol. 12183, 1218327 · © 2022 SPIE · 0277-786X · doi: 10.1117/12.2627942

Past imaging surveys were only sensitive to giant planets typically beyond 10 AU, in wide orbits.[5–7] Thanks to the VLTI infrastructure and the ongoing Gravity+ facility upgrade, Hi-5 will be well suited to push this semi-major upper limit to the snowline/iceline (around 2.7 AU for a solar-like star[8]). Radial velocity measurements have now established that there is a break in the giant planet occurrence rate in this region.[9,10] An overlapping between current radial velocity measurements and the Hi-5 measurements can lead to multiple detections and potential follow-up observations. In 2020, GRAVITY had already paved the way with the direct measurement of β Pictoris c, a radial velocity discovered planet orbiting at a distance of 2.7 AU from its star.[11] A sky survey, with a focus on the snowline region, is therefore proposed for the Hi-5 instrument.

Since planets in formation radiate more energy,[12] direct imaging surveys are keen to look at nearby young stellar systems ($<$ 250 Myr in age). Currently, two formation mechanisms are proposed to explain the formation of giant planets, cold-start (core accretion or "bottom-up") and hot-star (disk instability or "top-down"). The core accretion tends to be the most common formation mechanism for planetary-mass gas giants while larger objects, such as massive Jupiter-like planets and brown dwarfs, tend to form via gravitational instability in protoplanetary disks.[7,13–15] By measuring the luminosity of young planets, the formation model can be constrained. The rate of cooling depends on its initial conditions. Below 30 Myr, depending on the planet mass, the magnitude difference in the L' band is distinguishable and can lead to the distinction of the formation process.[12,16]

To assess a potential target list for the proposed survey, a list of 4002 stars, members of nearby ($<$ 150 pc) young stellar associations, is selected. This list was determined thanks to the BANYAN algorithm and other searches for young moving group members.[17] Around each of these stars, giant synthetic planets are generated and their magnitude is derived from the two formation models. The cold-start model used is the New Generation Planetary Population Synthesis (NGPPS), also known as the *Bern* model.[18] For the hot-start model, precomputed grids of model atmosphere, more precisely the AMES-Dusty model, are used. For this model, planets are generated according to the broken law derived by Fernandes et al. (2019) from past radial velocity surveys.[9]

The detection yield, based on the L-band planet's magnitude and position, is derived thanks to the SCIFYsim tools, an end-to-end simulator for the Hi-5 instrument (see Laugier et al. in this conference and in prep.). Multiple VLTI configurations and sub-selection on the catalog (star magnitude limit) are analyzed. Based on the results, an ordering of the stars is then performed.

The paper is organized as follows. Section 2 describes the stellar catalog. Section 3 is dedicated to the cold-start (Sec. 3.1) and hot-start (Sec. 3.2) formation model. In section 4, we present our end-to-end performance simulator tool, SCIFYsim, and how it is used to assessed the detectability of an exoplanet. Section 5 presents the results and the detection yield for both formation model. Our conclusions are presented in Section 6.

2. STELLAR CATALOGUE

Since the luminosity of giant exoplanets is age-dependent, young stellar systems are targeted for direct imaging. The formation model can be discriminated based on the received flux (magnitude).[12] Our stellar sample is therefore focused on nearby young (age $<$ 275 Myr and distance $<$ 150 pc) moving groups.

To determine the membership and create the stellar catalog, the *Gaia*'s second data release (DR2) was used, coupled with the BANYAN algorithm and other searches for young moving groups.[17] The probability of membership is based on the stellar coordinates, the distance (parallax measurement), and proper motion.

The exoplanet occurrence is directly related to the stellar mass,[10,19] which is taken into account in the modeling of the *Bern* model.[18,20] Protoplanetary disk mass increases with the stellar mass and so giant planets are more likely to form. There is a positive correlation between giant planet occurrence and stellar mass.[19] For the AMES-Dusty model (hot-start model), this phenomenon is implemented in the planets generator via a linear scaling following the stellar mass as done by Wallace et al. (2021).[12]

Mass estimates are based on spectral type–mass relations[21†], slightly modified in the case of pre-main-sequence stars, which tend to have a slightly larger mass for a fixed spectral type. In the substellar regime, sequences were extrapolated onto evolutionary sequences,[22] using spectral type–effective temperature sequences.[21,23] Their young sequences were used for ages below 200 Myr, and field sequences were used above this age. The spectral

[†]Available at https://www.pas.rochester.edu/~emamajek/EEM_dwarf_UBVIJHK_colors_Teff.txt

type-mass sequences at young ages deviate slightly in the G0–M5 range, where young stars are 15–25% more massive for a fixed spectral type; we adopted a log-linear deviation from the Pecault (2013) sequence anchored on the dynamical mass measurements of young stars in the literature,[21] which we updated using recent Gaia EDR3 parallax measurements when available.[20,24–31] The standard deviations of dynamical mass measurements around the Pecault (2013)[21] relations in log space were about 10% for both young and main-sequence stars, and we have adopted these for our mass estimation uncertainties in the relevant range of spectral types (M5 and earlier). In the case of later spectral types, our pre-main-sequence relation was extrapolated onto the $\leq$ 200 Myr Burrows (1993) models for which we adopted conservative 20% measurement errors to account for any possible model systematics.[22] Our main-sequence relation was similarly extrapolated onto the separate $>$ 200 Myr Burrows (1993) sequences also with 20% measurement errors. These mass estimates will be presented along with a database of young associations (Gagn et al., in prep.).

To estimate the mass of each individual star, we use a Monte Carlo simulation where we generate 10^4 synthetic spectral types in a Gaussian distribution centered on the available measurement and which standard deviation corresponds to the measurement error (usually 0.5 subtypes). Similarly, 10^4 synthetic ages are drawn following the age estimate of a star and its measurement error. Each synthetic spectral type and age data point is then transformed to an individual mass estimate using our empirical sequences; and the resulting median value of all synthetic masses in log space is taken as the best estimate, and the median absolute deviation in log space is taken as the contribution to our measurement error arising from the propagated spectral type and age measurement errors. We chose the median absolute deviation because it is more robust against outliers, or non-Gaussian distributions with long tails. We have added the errors associated with our sequences (10–20% depending on the spectral type) in quadrature to obtain our final mass estimate error. Our resulting mass uncertainties are larger than what can be done with individual M dwarfs by comparing their absolute K-band magnitude with empirical relations (e.g., see 32), however, doing so with a large catalog of young stars would be prone to systematic biases caused the age-dependent absolute K-band magnitude to mass and by unresolved binary stars. We, therefore, chose to use more conservative and less precise mass estimations that will be subject to fewer biases, until an analysis similar to Mann et al. (2019) is available for stars younger than $\approx$ 200 Myr and until we have a sample in which unresolved binaries are clearly identified.

2.1 Catalogue presentation

The full stellar catalog is composed of 5139 stars but is restricted to stars that are observable with the Auxiliary Telescopes (AT) from VLTI ($-80° < \delta < 16°$ in the most favorable case) and of spectral type 'M', 'G', 'K', 'F' or 'A'. With these constraints, the catalog is reduced to 4002 stars.

Figure 1 provides five histograms of target parameters. Cumulated and normalized distribution are available in Figure 9 in Appendix A. Approximately 65% of these stars have an age below 30 Myr. This value, represented with the green line, corresponds in the 'tuning fork' diagram in Wallace et al. (2021) to the age when the cooling of the planet prevents distinguishing cold from hot-start formation model.

Magnitudes in L' band (3.8 µm) are not directly available in the stellar catalog. It is computed thanks to the AllWISE catalog.[34] The catalog provides magnitude in four spectral channels, but only the two firsts, at 3.4 µm and 4.6 µm, are used. The magnitude at 3.8 µm is then linearly interpolated between these two values for each star. Measurements capabilities are mainly limited by the performance of NAOMI, the adaptive optics system of the ATs of the VLTI.[33] With this adaptive system, the limiting magnitude is $K = 9$ mag for GRAVITY and the performance should be similar in the L' band. This threshold (high Strehl regime requirement) is represented in Fig. 1 with a vertical red line. Around 40% of our stellar catalog has a lower magnitude. ASGARD should improve this threshold up to $K = 11.5$ (see Martinod et al in this conference).

All stars are situated in a range of 150 pc around the Earth, which allows the VLTI to have sufficient angular resolution to resolve the snowline (blue zone in Fig. 1). Two regimes are presented, one around 50 pc and the second one, with 2.5 more stars around 130 pc.

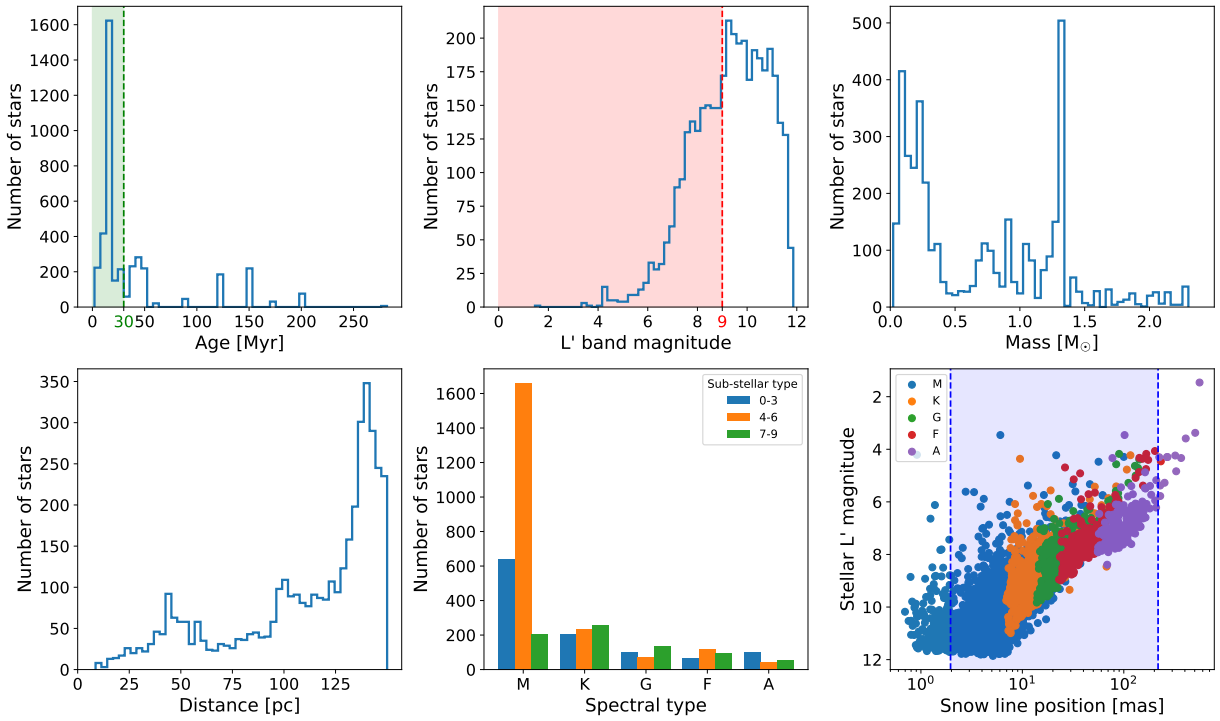

Figure 1: Age, L'-band magnitude, mass, distance, spectral-type, and snowline position distribution for our stellar catalog. The catalog is composed of 4002 stars. All of these stars are thought to be in young moving groups. The green vertical line in the age histogram corresponds to the planet/stellar age when the cooling of the planet prevents to distinguished cold from hot-start formation model.[12] The red vertical line in the magnitude histogram corresponds to the performance of NAOMI.[33] The blue zone in the snowline distribution represents the FoV of the ATs (IWA-OWA).

3. GIANT PLANETS FORMATION MODELS

3.1 Cold start model

3.1.1 Model presentation

The Generation III *Bern* model is a global model for planetary system formation. With the increase of known exoplanets, a model explaining how planets form and evolve is necessary. This model was developed a few years ago[35] and improved to now be able to follow the long-term evolution of multi-planetary systems, on gigayear timescales after formation.[18] For this survey, the focus is on young exoplanets but some stars have an age above 20 Myr (formation time) and this evolution modeling is important.

The *Bern* model starts with a small number of embryos (50) in the planetesimal disc. Then, embryos accrete solids and gas to form protoplanets until the rate becomes greater than what the disc can provide.[18] Migration of planets is considered, as well as interactions or collisions between protoplanets. After 20 Myr, the main formation phase is over and an evolutionary phase, until 10 Gyr, begins.[18] Being a core-accretion model (a.k.a. cold-start model), giant planets are cooler (less bright) than hot-start model at formation.[18]

To increase the statistical confidence in the model, it is run 1000 times, providing up to 1000 potential planetary systems. At each time step, information about the planets can be recovered (mass, radius, orbital position) and these planets can be injected in SCIFYsim sensitivity map. The apparent magnitudes in L'-band have been computed thanks to a black-body assumption at the planet temperature. This temperature is derived from the planet's bolometric luminosity and radius provided by the model.

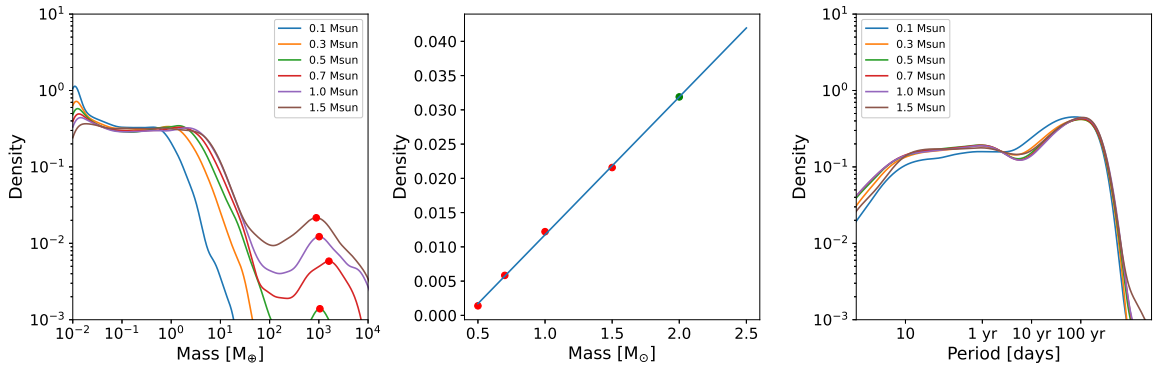

Figure 2: LEFT: Kernel-density estimate of planetary mass distribution (30 Myr) for cold-start planets. Based on Figure 10 from Burn et al. (2021).[20] CENTER: Kernel-density at the peak (red dot) in the 10^2 $M_\oplus - 10^4$ $M_\oplus$ range. The blue line is a linear interpolation between these dots. Green dot is an estimate of the peak density for a 2.0 $M_\odot$ star. RIGHT: Kernel-density estimate of planetary period distribution for different stellar masses (30 Myr) for cold-start planets.

3.1.2 Stellar mass influence

First focused on solar-type stars and how planetary populations evolve in comparison to our solar system, this model is also extended to low-mass stars.[20,36] Due to the complexity and computation time needed, results were tabulated for specific stellar masses (0.1 $M_\odot$, 0.3 $M_\odot$, 0.5 $M_\odot$, 0.7 $M_\odot$ and 1.0 $M_\odot$).[20] Unpublished table, for 1.5 $M_\odot$, is used in this paper to increase the range of stellar masses. Margins are considered, and for instance, each star with a 0.2 $M_\odot - 0.4$ $M_\odot$ mass uses the precomputed results for 0.3 $M_\odot$, and so on. Our analysis around these stars is therefore limited to a maximal stellar mass of 1.75 $M_\odot$.

In Burn et al (2021), the Fig. 10 shows that the density of giant planets (above 10^2 $M_\oplus$) is null for low-mass stars and increases for larger stellar mass.[20] This figure is reproduced (Fig. 2) and enhanced with the new set of data (1.5 $M_\odot$). The peak value, in the 10^2 $M_\oplus - 10^4$ $M_\oplus$ region, increases linearly. The density for higher stellar mass could be linearly interpolated up to 2 $M_\odot$ (green dot). Above this value, RV surveys tend to indicate that the density of giant planets decreases.[37] Moreover, disk morphology and disk photo-evaporation could have an impact and are not included in the model. In Fig. 1, the second peak in the stellar mass histogram is below 2 $M_\odot$ and 90% of stars have a mass below this value. Interpolation was therefore not performed since most of the stellar mass is already captured by the available stellar masses.

3.2 Hot start model

3.2.1 Planets generation

Contrary to the *Bern* model, hot-star model does not provide a full catalog of planets. It only provides precomputed grids of model atmosphere. The planets' parameters (mass, period) should be generated with an external model. Planets are therefore generated from statistics with an empirical law. We used the well-known Fernandes power-law distribution.[9] This fitting law shows that there is a turnover in the radial-velocity curve at an orbital period, which can be related to a specific angular separation or semi-major axis if a circular orbit is assumed. Depending on the fitting parameter, the turnover changes slightly but it is located near the snowline region. The Fulton power-law distribution law[10] or synthetic populations (Forgan et al. 2018) could be used in the future.[38]

We generated planets with a mass between 30 to 6000 $M_\oplus$ (0.01 to 19 M_{jup}) and a period between 10 to 10000 days. The number of planets around a specific star follows a Poisson law. A linear scaling factor was added to take into account the stellar mass influence ($C = M_*/M_\odot$), increasing the number of planets for larger stars. The stellar age is not a parameter for the planet generation, contrary to the *Bern* model. The inclination is randomized per planetary system, i.e. each planet has the same inclination for a specific star. As for the cold

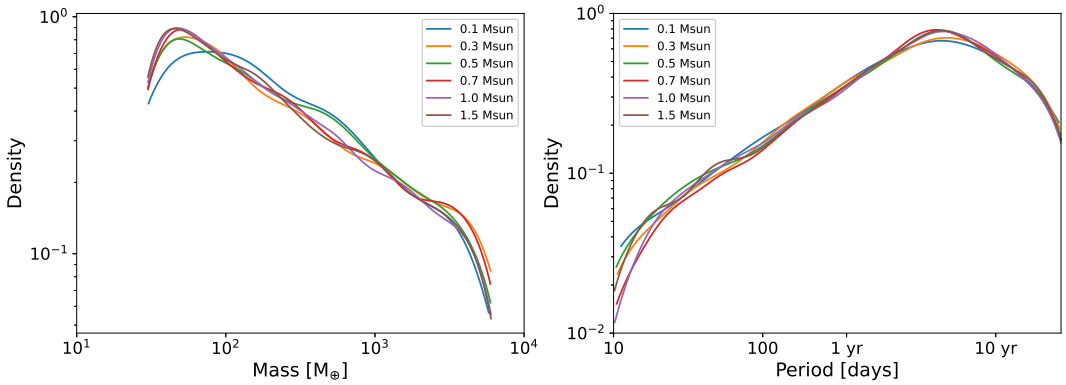

Figure 3: LEFT: Kernel-density estimate of planetary mass distribution for different stellar masses (hot-star planets). RIGHT: Kernel-density estimate of planetary period distribution for different stellar masses. The Fernandes power-law distribution is used.[9] The turnover is clearly visible.

start model, to increase the statistical confidence, the planet generation is run 1000 times, providing up to 1000 potential planetary systems.

Figure 3 shows the Kernel-density estimate for the model (mass and period). The turnover is clearly visible. Contrary to the *Bern* model, the scaling with the stellar mass is less present. The overall density of giant planets is higher, with nearly a factor of ten between both models.

3.2.2 Magnitude computation

Hot-start model is based on the disk instability (or "top-down") approach. For the planet magnitude, needed for the detection test, we used the AMES-Dusty model.[39,40] These are pre-computed grids of model atmosphere and isochrones for low-mass stars and brown dwarfs[‡]. AMES refers to the water vapor line and Dusty means that the dust content is maximum (dust is formed in equilibrium with the gas phase).

Isochrones provide the planet magnitude for a specific age and mass ratio (planet mass/stellar mass). The WISE filters, so the same as for the stellar magnitudes (see Sec. 2), are available. As previously, W_1 and W_2 filters (3.4 µm and 4.6 µm) are used and the magnitude at 3.8 µm is linearly interpolated. Since isochrones are tabulated values, an interpolation (linear) is necessary to get the magnitude values at the right planet mass and age. Planets are considered as old as their parent star.

4. END-TO-END PERFORMANCE SIMULATOR TOOL

SCIFYSIM is an end-to-end simulator for single-mode filtered interferometers, with an emphasis on nulling beam-combiners. The main focus is the Hi-5 instrument. It provides sensitivity maps in the field of view based on advanced hypothesis testing techniques. A full description of the tool is presented at this conference (Laugier et al. + submitted).

The tool is used as follows. Sensitivity maps (Fig. 4) are precomputed for both UTs and ATs with a fixed integration time. The goal is to do a survey of stars (follow-up of stars with a Gaia acceleration). ATs are selected, as well as the lowest resolution mode ($R = 20$) of the instrument (see Dandumont et al. at this conference + in prep.). These maps provide information on the planet's magnitude sensitivity depending on the star magnitude, the star declination, the planet's relative position, and the configuration of the four telescopes. Several AT configurations ("small", "medium", "large" and "astrometric") are available and the order of recombination between the four telescopes can also vary (e.g. large [0 1 2 3] vs. large [0 3 1 2]).[§] All of these parameters have of course a direct impact on the transmission map and so on the presented sensitivity maps.

[‡]Available at https://phoenix.ens-lyon.fr/Grids/README

[§]http://www.eso.org/sci/facilities/paranal/telescopes/vlti/configuration/P110.html

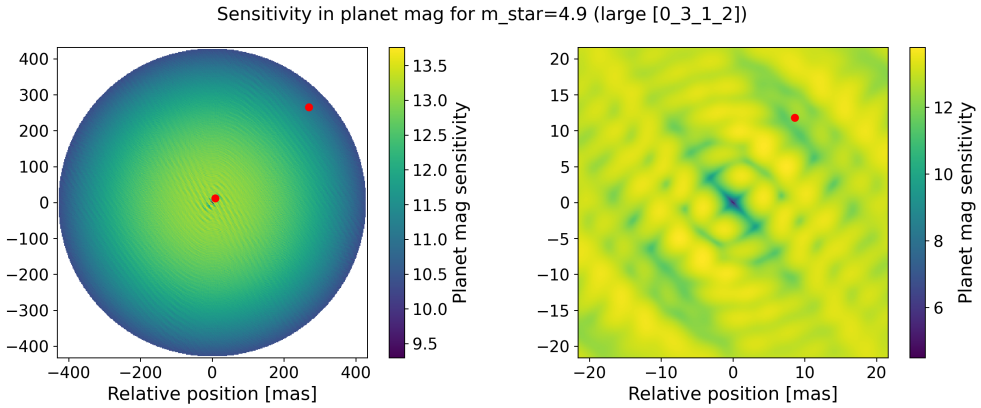

Figure 4: Sensitivity map computed by SCIFYSIM for a 4.9-mag stars with the AT ($R = 20$) and the "large" configuration ([0 3 1 2]). Both red dots correspond to randomized planets. LEFT: full field of view. RIGHT: zoom and more detailed sensitivity map.

For illustration, Fig. 4 represents the sensitivity map for a 4.9-mag star with a declination of −23.3 deg. The ATs are used with the large configuration (order of telescope recombination: [0 3 1 2]) and a spectral resolution $R = 20$. Two planets are randomly positioned, one near the center (inner planet) and one far away from the star. If the planet's magnitude is below this sensitivity, it is considered as detected. In this case, it corresponds to a contrast of around 10^{-4} (see Laugier et al.).

The configuration will mainly affect the zone near the star (influence of the transmission map and the spatial resolution). The small configuration provides, obviously, a degraded angular resolution.

5. RESULTS

5.1 Cold start model

As explained in Sect. 3.1.2, the occurrence of sub-giant and giant planets is low and depends on the stellar mass. Figure 2 shows that the density for low-mass stars in the cold-start case is closed to 0 and is 0.02 for a 1.5 $M_\odot$ star. Burn et al (2021) gives the fraction of systems with specific planetary types for the different stellar mass populations (Tab. 3).[20] It shows that the fraction of sub-giants and giants increases with the stellar mass and is resp. 0.05 and 0.19 for a 1.0 $M_\odot$ star.

Unfortunately, only massive planets tend to have a magnitude low enough to be detected by Hi-5. Figure 5a presents a histogram of the L' band magnitude of planets for a specific star ($M = 1.3$ $M_\odot$ star). Only planets with a mass of at least 0.75 M_{jup} are shown for computational efficiency. As illustrated with the sensitivity map (Fig. 4), Hi-5 is sensitive to planets with a magnitude below 12-13. Our simulations show that no planet, with the cold-start model, can be detected. In fact, cold-star planets are indeed too cold and massive planets are too scarce.

5.2 Hot start model

For the hot start model, the occurrence of giant planets is higher. Moreover, due to the formation process, hot star planets are brighter at young ages than cold start planets. Figure 5b presents an histogram of the planet magnitudes. The same star as for the *Bern*-model (Fig. 5a) is used. Magnitudes are clearly lower, which means that planets are brighter. It leads to numerous detections.

Figure 6 shows the cumulative detection yield for the numerous baseline configurations as a function of the number of stars in the survey. The stars are ordered from the highest detections to the lowest. As expected, some stars (distant, old, and low-mass stars) are less favorable to having detectable planets. Our survey will of course be limited to a few dozens of stars and not the full catalog. This figure is therefore important and shows nearly a linear trend at the beginning (the figure is in log-scale). This linear trend tends to demonstrate that

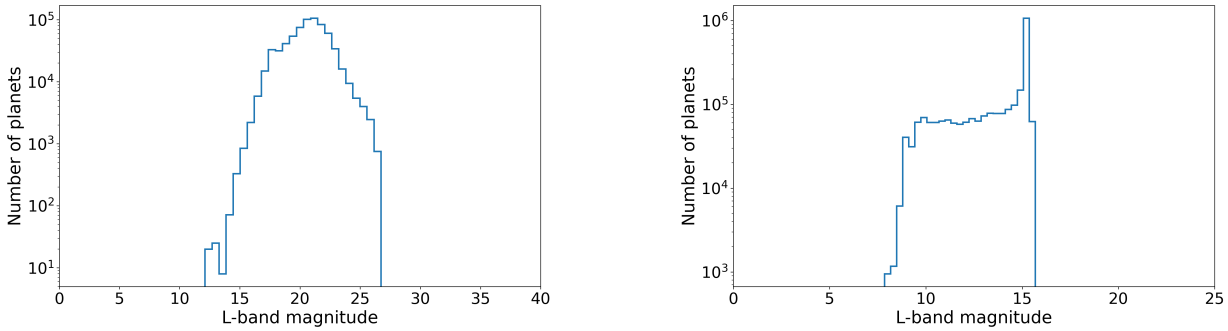

(a) *Bern*-model. $M_{\rm pl} > 0.75\ M_{\rm jup}$ (b) Hot start model.

Figure 5: Histogram of the L' band magnitude of planets generated (1000 simulations with 50 embryos) around a 1.3 $M_\odot$ star.

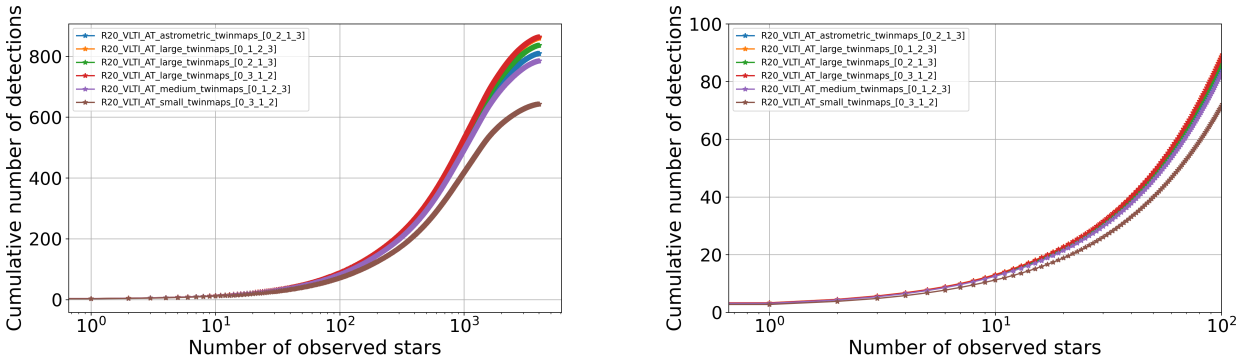

(a) Full stellar catalog. (b) Truncated at the 100 first stars.

Figure 6: Cumulative number of detections for different VLTI configurations (ATs). Stars are ordered by the number of detections. Hot-star model (AMES-Dusty model) with the Fernandes law (planet generation) is used. SCIFYSIM is used to asses the detectability.

the survey is not yet optimized. The integration time could be a degree of freedom. The baseline configurations have a very low effect on these stars but large configurations should nevertheless be used to maximize the chance of detection.

One important aspect is to know exactly what type of planets are detected. Figure 7 shows the distribution and occurrence of detected exoplanets (whole catalog) for one baseline configuration ("large" [0 3 1 2]). Hi-5 detects mainly giant planets (> 2 $M_{\rm jup}$) located around the snow line, which is consistent with the Fernandes law.

It is also interesting to constrain in mass the systems that Hi-5 is observing. Figure 8 provides the percentage of detections as a function of the mass and the stellar insolation. It proves that our instrument is able to detect more than 80% of planets with a mass above 10 $M_{\rm jup}$ and 50% of planets with $M > 4$ $M_{\rm jup}$. As expected, 1.5 $M_{\rm jup}$ is a limit of detections for the instrument. This figure also means that Hi-5 will be able to discriminate the formation model since cold-start model tends to not form very massive planets.

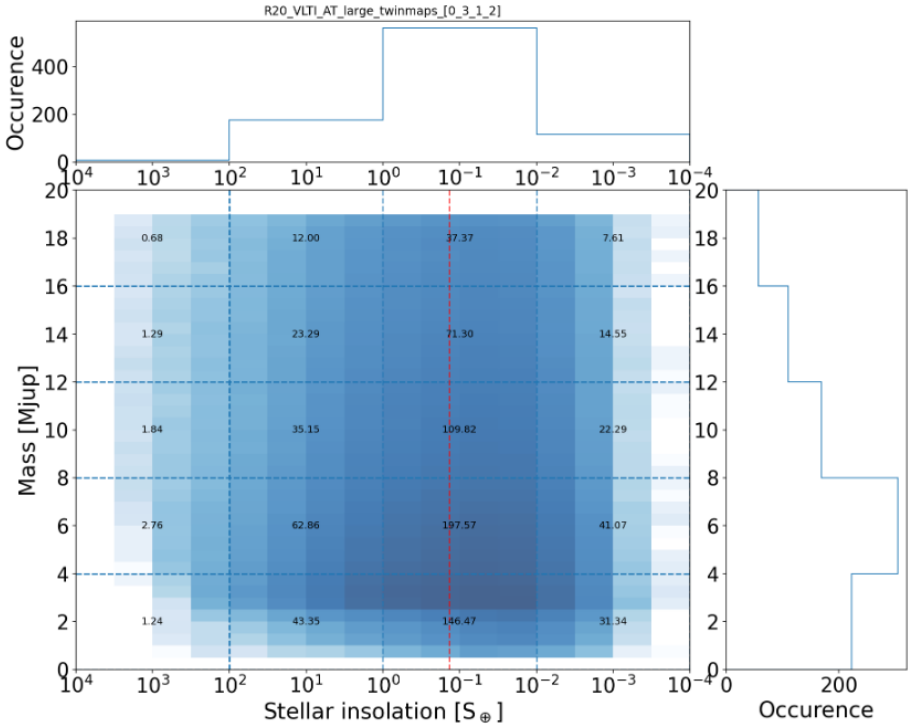

Figure 7: Number of exoplanets detected around the full catalog (4002 stars) with the Hi-5 instrument and the associated occurrences. Hot-stat model (AMES-Dusty model + Fernandes law) with the large configuration of the ATs ($R = 20$). The red dotted line represents the snow line position.

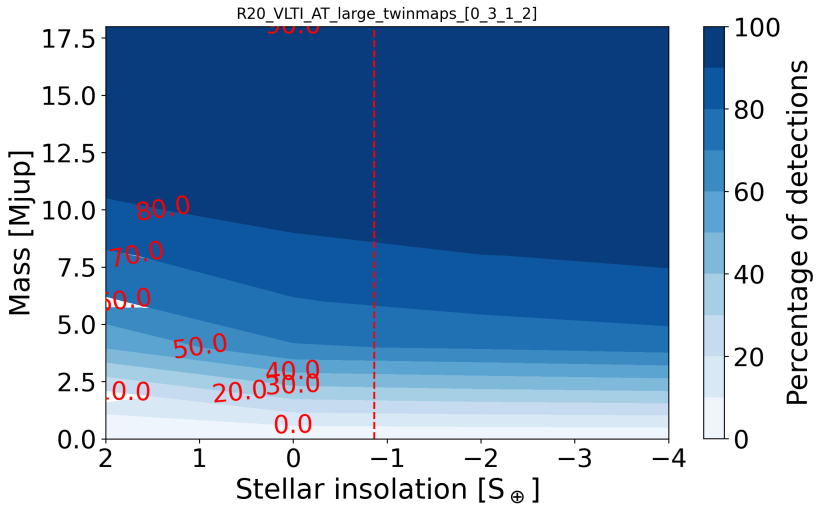

Figure 8: Percentage of detections around the full catalog (4002 stars) as a function of the mass and the stellar insolation. Hot-stat model (AMES-Dusty model + Fernandes law) with the large configuration of the ATs ($R = 20$). The red dotted line represents the snow line position.

6. CONCLUSION

We investigated the detection yield of the ASGARD/Hi-5 instrument. It is a proposed high-contrast nulling interferometer for the Very Large Telescope (VLTI) and it operates in L'-band. Its scientific focus is on giant exoplanets characterization and formation, protoplanetary disks around young stars, and the prevalence and nature of exozodiacal dust.

A survey of nearby young stars is planned with the ATs ($R = 20$). A catalog of 4002 stars is used to derive the target list. The stars are identified as members of young stellar associations (65% have an age $<$ 30 Myr). Around each of these stars, synthetic exoplanet systems are generated. Two formation modes are used, a cold-start one (*Bern*-model) and a hot-start one (AMES-Dusty). Thanks to SCIFYsim, our an end-to-end simulator of the Hi-5 instrument, we are able to compute the detection yield.

The instrument is insensitive to cold-start planets, these planets being too small and not bright enough. On the contrary, our yield computation shows that Hi-5 is able to detect more than 50% of the hot-start planets with a mass larger than M $>$ 4 M_{jup}. With the large AT configuration, more than 40 planets could be detected assuming 20 nights of observations and two stars per night.

Further work will include optimization of the observation strategy (integration time per target, Zenith distance) and a target list. Another model for hot-start planets (Forgan) will also be investigated.

APPENDIX A. APPENDIX

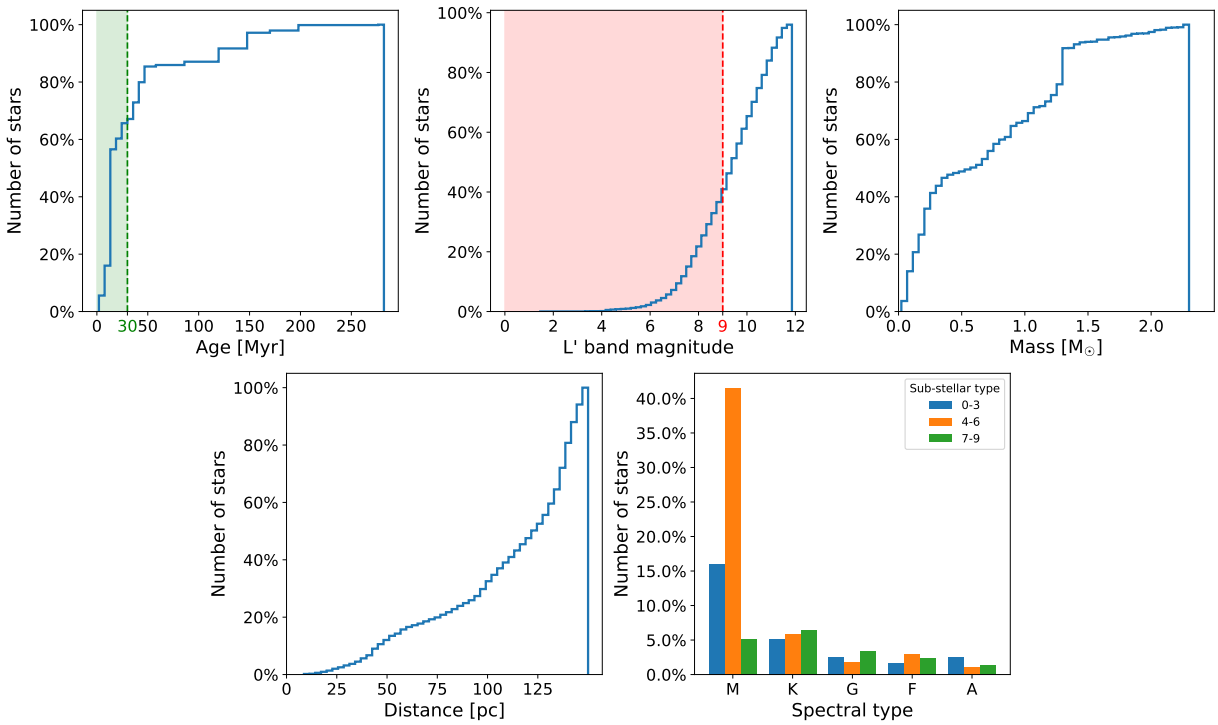

Figure 9: Age, L'-band magnitude, mass, distance, and spectral-type cumulated (and normalized) distribution for our stellar catalog. The catalog is composed of 4002 stars. All of these stars are thought to be in young moving groups. The green vertical line in the age histogram corresponds to the planet/stellar age when the cooling of the planet prevents to distinguished cold from hot-start formation model.[12] The red vertical line in the magnitude histogram corresponds to the performance of NAOMI.[33]

ACKNOWLEDGMENTS

Author contributions: CD carried out the analyses and wrote the manuscript. A.E provided the *Bern*-model data. J.G. provided the stellar catalog and wrote the section about it. RL developed SCIFYsim. JL and DD initiated and guided this project. All authors discussed the results and commented on the manuscript. SCIFY has received funding from the European Research Council (ERC) under the European Union's Horizon 2020 research and innovation program (grant agreement CoG - 866070). This project has received funding from the European Unions Horizon 2020 research and innovation programme under grant agreement No 101004719.

REFERENCES

[1] Mayor, M. and Queloz, D., "A Jupiter-mass companion to a solar-type star," *Nature* **378**, 355–359 (Nov. 1995).

[2] Bowens, R., Meyer, M. R., Delacroix, C., Absil, O., van Boekel, R., Quanz, S. P., Shinde, M., Kenworthy, M., Carlomagno, B., Orban de Xivry, G., Cantalloube, F., and Pathak, P., "Exoplanets with ELT-METIS: I. Estimating the direct imaging exoplanet yield around stars within 6.5 parsecs," *Astronomy & Astrophysics* **653**, A8 (Sept. 2021).

[3] Quanz, S. P., Ottiger, M., Fontanet, E., Kammerer, J., Menti, F., Dannert, F., Gheorghe, A., Absil, O., Airapetian, V. S., Alei, E., Allart, R., Angerhausen, D., Blumenthal, S., Buchhave, L. A., Cabrera, J., Carrion-Gonzalez, ., Chauvin, G., Danchi, W. C., Dandumont, C., Defrre, D., Dorn, C., Ehrenreich, D.,

Ertel, S., Fridlund, M., Muoz, A. G., Gascn, C., Girard, J. H., Glauser, A., Grenfell, J. L., Guidi, G., Hagelberg, J., Helled, R., Ireland, M. J., Kopparapu, R. K., Korth, J., Kozakis, T., Kraus, S., Lger, A., Leedjrv, L., Lichtenberg, T., Lillo-Box, J., Linz, H., Liseau, R., Loicq, J., Mahendra, V., Malbet, F., Mathew, J., Mennesson, B., Meyer, M. R., Mishra, L., Molaverdikhani, K., Noack, L., Oza, A. V., Pall, E., Parviainen, H., Quirrenbach, A., Rauer, H., Ribas, I., Rice, M., Romagnolo, A., Rugheimer, S., Schwieterman, E. W., Serabyn, E., Sharma, S., Stassun, K. G., Szulgyi, J., Wang, H. S., Wunderlich, F., Wyatt, M. C., and collaboration, t. L., "Large Interferometer For Exoplanets (LIFE): I. Improved exoplanet detection yield estimates for a large mid-infrared space-interferometer mission," *arXiv:2101.07500 [astro-ph]* (May 2021). arXiv: 2101.07500.

[4] Defrre, D., Absil, O., Berger, J.-P., Boulet, T., Danchi, W. C., Ertel, S., Gallenne, A., Hnault, F., Hinz, P., Huby, E., Ireland, M., Kraus, S., Labadie, L., Le Bouquin, J.-B., Martin, G., Matter, A., Mrand, A., Mennesson, B., Minardi, S., Monnier, J. D., Norris, B., de Xivry, G. O., Pedretti, E., Pott, J.-U., Reggiani, M., Serabyn, E., Surdej, J., Tristram, K. R. W., and Woillez, J., "The path towards high-contrast imaging with the VLTI: the Hi-5 project," *Experimental Astronomy* **46**, 475–495 (Dec. 2018).

[5] Stone, J. M., Skemer, A. J., Hinz, P. M., Bonavita, M., Kratter, K. M., Maire, A.-L., Defrere, D., Bailey, V. P., Spalding, E., Leisenring, J. M., Desidera, S., Bonnefoy, M., Biller, B., Woodward, C. E., Henning, T., Skrutskie, M. F., Eisner, J. A., Crepp, J. R., Patience, J., Weigelt, G., De Rosa, R. J., Schlieder, J., Brandner, W., Apai, D., Su, K., Ertel, S., Ward-Duong, K., Morzinski, K. M., Schertl, D., Hofmann, K.-H., Close, L. M., Brems, S. S., Fortney, J. J., Oza, A., Buenzli, E., and Bass, B., "The LEECH Exoplanet Imaging Survey: Limits on Planet Occurrence Rates Under Conservative Assumptions," *The Astronomical Journal* **156**, 286 (Nov. 2018). arXiv: 1810.10560.

[6] Vigan, A., Fontanive, C., Meyer, M., Biller, B., Bonavita, M., Feldt, M., Desidera, S., Marleau, G.-D., Emsenhuber, A., Galicher, R., Rice, K., Forgan, D., Mordasini, C., Gratton, R., Le Coroller, H., Maire, A.-L., Cantalloube, F., Chauvin, G., Cheetham, A., Hagelberg, J., Lagrange, A.-M., Langlois, M., Bonnefoy, M., Beuzit, J.-L., Boccaletti, A., DOrazi, V., Delorme, P., Dominik, C., Henning, T., Janson, M., Lagadec, E., Lazzoni, C., Ligi, R., Menard, F., Mesa, D., Messina, S., Moutou, C., Mller, A., Perrot, C., Samland, M., Schmid, H. M., Schmidt, T., Sissa, E., Turatto, M., Udry, S., Zurlo, A., Abe, L., Antichi, J., Asensio-Torres, R., Baruffolo, A., Baudoz, P., Baudrand, J., Bazzon, A., Blanchard, P., Bohn, A. J., Brown Sevilla, S., Carbillet, M., Carle, M., Cascone, E., Charton, J., Claudi, R., Costille, A., De Caprio, V., Delboulb, A., Dohlen, K., Engler, N., Fantinel, D., Feautrier, P., Fusco, T., Gigan, P., Girard, J. H., Giro, E., Gisler, D., Gluck, L., Gry, C., Hubin, N., Hugot, E., Jaquet, M., Kasper, M., Le Mignant, D., Llored, M., Madec, F., Magnard, Y., Martinez, P., Maurel, D., Mller-Nilsson, O., Mouillet, D., Moulin, T., Orign, A., Pavlov, A., Perret, D., Petit, C., Pragt, J., Puget, P., Rabou, P., Ramos, J., Rickman, E. L., Rigal, F., Rochat, S., Roelfsema, R., Rousset, G., Roux, A., Salasnich, B., Sauvage, J.-F., Sevin, A., Soenke, C., Stadler, E., Suarez, M., Wahhaj, Z., Weber, L., and Wildi, F., "The SPHERE infrared survey for exoplanets (SHINE): III. The demographics of young giant exoplanets below 300 au with SPHERE," *Astronomy & Astrophysics* **651**, A72 (July 2021).

[7] Nielsen, E. L., De Rosa, R. J., Macintosh, B., Wang, J. J., Ruffio, J.-B., Chiang, E., Marley, M. S., Saumon, D., Savransky, D., Mark Ammons, S., Bailey, V. P., Barman, T., Blain, C., Bulger, J., Burrows, A., Chilcote, J., Cotten, T., Czekala, I., Doyon, R., Duchne, G., Esposito, T. M., Fabrycky, D., Fitzgerald, M. P., Follette, K. B., Fortney, J. J., Gerard, B. L., Goodsell, S. J., Graham, J. R., Greenbaum, A. Z., Hibon, P., Hinkley, S., Hirsch, L. A., Hom, J., Hung, L.-W., Ilene Dawson, R., Ingraham, P., Kalas, P., Konopacky, Q., Larkin, J. E., Lee, E. J., Lin, J. W., Maire, J., Marchis, F., Marois, C., Metchev, S., Millar-Blanchaer, M. A., Morzinski, K. M., Oppenheimer, R., Palmer, D., Patience, J., Perrin, M., Poyneer, L., Pueyo, L., Rafikov, R. R., Rajan, A., Rameau, J., Rantakyr, F. T., Ren, B., Schneider, A. C., Sivaramakrishnan, A., Song, I., Soummer, R., Tallis, M., Thomas, S., Ward-Duong, K., and Wolff, S., "The Gemini Planet Imager Exoplanet Survey: Giant Planet and Brown Dwarf Demographics from 10 to 100 au," *The Astronomical Journal* **158**, 13 (June 2019).

[8] Ida, S. and Lin, D. N. C., "Toward a Deterministic Model of Planetary Formation. III. Mass Distribution of ShortPeriod Planets around Stars of Various Masses," *The Astrophysical Journal* **626**, 1045–1060 (June 2005).

[9] Fernandes, R. B., Mulders, G. D., Pascucci, I., Mordasini, C., and Emsenhuber, A., "Hints for a Turnover at the Snow Line in the Giant Planet Occurrence Rate," *The Astrophysical Journal* **874**, 81 (Mar. 2019).

[10] Fulton, B. J., Rosenthal, L. J., Hirsch, L. A., Isaacson, H., Howard, A. W., Dedrick, C. M., Sherstyuk, I. A., Blunt, S. C., Petigura, E. A., Knutson, H. A., Behmard, A., Chontos, A., Crepp, J. R., Crossfield, I. J. M., Dalba, P. A., Fischer, D. A., Henry, G. W., Kane, S. R., Kosiarek, M., Marcy, G. W., Rubenzahl, R. A., Weiss, L. M., and Wright, J. T., "California Legacy Survey. II. Occurrence of Giant Planets beyond the Ice Line," *The Astrophysical Journal Supplement Series* **255**, 14 (July 2021).

[11] Nowak, M., Lacour, S., Lagrange, A.-M., Rubini, P., Wang, J., Stolker, T., Abuter, R., Amorim, A., Asensio-Torres, R., Baubck, M., Benisty, M., Berger, J. P., Beust, H., Blunt, S., Boccaletti, A., Bonnefoy, M., Bonnet, H., Brandner, W., Cantalloube, F., Charnay, B., Choquet, E., Christiaens, V., Clnet, Y., Coud du Foresto, V., Cridland, A., de Zeeuw, P. T., Dembet, R., Dexter, J., Drescher, A., Duvert, G., Eckart, A., Eisenhauer, F., Gao, F., Garcia, P., Garcia Lopez, R., Gardner, T., Gendron, E., Genzel, R., Gillessen, S., Girard, J., Grandjean, A., Haubois, X., Heiel, G., Henning, T., Hinkley, S., Hippler, S., Horrobin, M., Houll, M., Hubert, Z., Jimnez-Rosales, A., Jocou, L., Kammerer, J., Kervella, P., Keppler, M., Kreidberg, L., Kulikauskas, M., Lapeyrre, V., Le Bouquin, J.-B., Lna, P., Mrand, A., Maire, A.-L., Mollire, P., Monnier, J. D., Mouillet, D., Mller, A., Nasedkin, E., Ott, T., Otten, G., Paumard, T., Paladini, C., Perraut, K., Perrin, G., Pueyo, L., Pfuhl, O., Rameau, J., Rodet, L., Rodrguez-Coira, G., Rousset, G., Scheithauer, S., Shangguan, J., Stadler, J., Straub, O., Straubmeier, C., Sturm, E., Tacconi, L. J., van Dishoeck, E. F., Vigan, A., Vincent, F., von Fellenberg, S. D., Ward-Duong, K., Widmann, F., Wieprecht, E., Wiezorrek, E., Woillez, J., and the GRAVITY Collaboration, "Direct confirmation of the radial-velocity planet β Pictoris c," *Astronomy & Astrophysics* **642**, L2 (Oct. 2020).

[12] Wallace, A. L., Ireland, M. J., and Federrath, C., "Constraints on planets in nearby young moving groups detectable by high-contrast imaging and *Gaia* astrometry," *Monthly Notices of the Royal Astronomical Society* **508**, 2515–2523 (Oct. 2021).

[13] Rosenthal, L. J., Fulton, B. J., Hirsch, L. A., Isaacson, H. T., Howard, A. W., Dedrick, C. M., Sherstyuk, I. A., Blunt, S. C., Petigura, E. A., Knutson, H. A., Behmard, A., Chontos, A., Crepp, J. R., Crossfield, I. J. M., Dalba, P. A., Fischer, D. A., Henry, G. W., Kane, S. R., Kosiarek, M., Marcy, G. W., Rubenzahl, R. A., Weiss, L. M., and Wright, J. T., "The California Legacy Survey I. A Catalog of 178 Planets from Precision Radial Velocity Monitoring of 719 Nearby Stars over Three Decades," *The Astrophysical Journal Supplement Series* **255**, 8 (July 2021). arXiv: 2105.11583.

[14] Bowler, B. P., Blunt, S. C., and Nielsen, E. L., "Population-level Eccentricity Distributions of Imaged Exoplanets and Brown Dwarf Companions: Dynamical Evidence for Distinct Formation Channels," *The Astronomical Journal* **159**, 63 (Jan. 2020).

[15] Currie, T., Lawson, K., Schneider, G., Lyra, W., Wisniewski, J., Grady, C., Guyon, O., Tamura, M., Kotani, T., Kawahara, H., Brandt, T., Uyama, T., Muto, T., Dong, R., Kudo, T., Hashimoto, J., Fukagawa, M., Wagner, K., Lozi, J., Chilcote, J., Tobin, T., Groff, T., Ward-Duong, K., Januszewski, W., Norris, B., Tuthill, P., van der Marel, N., Sitko, M., Deo, V., Vievard, S., Jovanovic, N., Martinache, F., and Skaf, N., "Images of embedded Jovian planet formation at a wide separation around AB Aurigae," *Nature Astronomy* (Apr. 2022).

[16] Spiegel, D. S. and Burrows, A., "SPECTRAL AND PHOTOMETRIC DIAGNOSTICS OF GIANT PLANET FORMATION SCENARIOS," *The Astrophysical Journal* **745**, 174 (Feb. 2012).

[17] Gagn, J., Mamajek, E. E., Malo, L., Riedel, A., Rodriguez, D., Lafrenire, D., Faherty, J. K., Roy-Loubier, O., Pueyo, L., Robin, A. C., and Doyon, R., "BANYAN. XI. The BANYAN Multivariate Bayesian Algorithm to Identify Members of Young Associations with 150 pc," *ApJ* **856**, 23 (Mar. 2018).

[18] Emsenhuber, A., Mordasini, C., Burn, R., Alibert, Y., Benz, W., and Asphaug, E., "The New Generation Planetary Population Synthesis (NGPPS). I. Bern global model of planet formation and evolution, model tests, and emerging planetary systems," *Astronomy & Astrophysics* **656**, A69 (Dec. 2021). arXiv: 2007.05561.

[19] Mulders, G. D., "Planet Populations as a Function of Stellar Properties," *arXiv:1805.00023 [astro-ph]* , 1–26 (2018). arXiv: 1805.00023.

[20] Burn, R., Schlecker, M., Mordasini, C., Emsenhuber, A., Alibert, Y., Henning, T., Klahr, H., and Benz, W., "The New Generation Planetary Population Synthesis (NGPPS). IV. Planetary systems around low-mass stars," *Astronomy & Astrophysics* **656**, A72 (Dec. 2021). arXiv: 2105.04596.

[21] Pecaut, M. J. and Mamajek, E. E., "INTRINSIC COLORS, TEMPERATURES, AND BOLOMETRIC CORRECTIONS OF PRE-MAIN-SEQUENCE STARS," *The Astrophysical Journal Supplement Series* **208**, 9 (Sept. 2013).

[22] Burrows, A., Hubbard, W. B., Saumon, D., and Lunine, J. I., "An expanded set of brown dwarf and very low mass star models," *The Astrophysical Journal* **406**, 158 (Mar. 1993).

[23] Filippazzo, J. C., Rice, E. L., Faherty, J., Cruz, K. L., Van Gordon, M. M., and Looper, D. L., "FUNDAMENTAL PARAMETERS AND SPECTRAL ENERGY DISTRIBUTIONS OF YOUNG AND FIELD AGE OBJECTS WITH MASSES SPANNING THE STELLAR TO PLANETARY REGIME," *The Astrophysical Journal* **810**, 158 (Sept. 2015).

[24] Hillenbrand, L. A. and White, R. J., "An Assessment of Dynamical Mass Constraints on PreMainSequence Evolutionary Tracks," *The Astrophysical Journal* **604**, 741–757 (Apr. 2004).

[25] Rodet, L., Bonnefoy, M., Durkan, S., Beust, H., Lagrange, A.-M., Schlieder, J. E., Janson, M., Grandjean, A., Chauvin, G., Messina, S., Maire, A.-L., Brandner, W., Girard, J., Delorme, P., Biller, B., Bergfors, C., Lacour, S., Feldt, M., Henning, T., Boccaletti, A., Le Bouquin, J.-B., Berger, J.-P., Monin, J.-L., Udry, S., Peretti, S., Segransan, D., Allard, F., Homeier, D., Vigan, A., Langlois, M., Hagelberg, J., Menard, F., Bazzon, A., Beuzit, J.-L., Delboulb, A., Desidera, S., Gratton, R., Lannier, J., Ligi, R., Maurel, D., Mesa, D., Meyer, M., Pavlov, A., Ramos, J., Rigal, R., Roelfsema, R., Salter, G., Samland, M., Schmidt, T., Stadler, E., and Weber, L., "Dynamical masses of M-dwarf binaries in young moving groups: I. The case of TWA 22 and GJ 2060," *Astronomy & Astrophysics* **618**, A23 (Oct. 2018).

[26] Janson, M., Durkan, S., Bonnefoy, M., Rodet, L., Khler, R., Lacour, S., Brandner, W., Henning, T., and Girard, J., "Dynamical masses of M -dwarf binaries in young moving groups: II. Toward empirical mass-luminosity isochrones," *Astronomy & Astrophysics* **620**, A33 (Dec. 2018).

[27] Azulay, R., Guirado, J. C., Marcaide, J. M., Mart-Vidal, I., Ros, E., Tognelli, E., Jauncey, D. L., Lestrade, J.-F., and Reynolds, J. E., "The AB Doradus system revisited: The dynamical mass of AB Dor A/C," *Astronomy & Astrophysics* **607**, A10 (2017).

[28] Montet, B. T., Bowler, B. P., Shkolnik, E. L., Deck, K. M., Wang, J., Horch, E. P., Liu, M. C., Hillenbrand, L. A., Kraus, A. L., and Charbonneau, D., "DYNAMICAL MASSES OF YOUNG M DWARFS: MASSES AND ORBITAL PARAMETERS OF GJ 3305 AB, THE WIDE BINARY COMPANION TO THE IMAGED EXOPLANET HOST 51 ERI," *The Astrophysical Journal* **813**, L11 (Oct. 2015).

[29] Nielsen, E. L., Rosa, R. J. D., Wang, J., Rameau, J., Song, I., Graham, J. R., Macintosh, B., Ammons, M., Bailey, V. P., Barman, T. S., Bulger, J., Chilcote, J. K., Cotten, T., Doyon, R., Duchne, G., Fitzgerald, M. P., Follette, K. B., Greenbaum, A. Z., Hibon, P., Hung, L.-W., Ingraham, P., Kalas, P., Konopacky, Q. M., Larkin, J. E., Maire, J., Marchis, F., Marley, M. S., Marois, C., Metchev, S., Millar-Blanchaer, M. A., Oppenheimer, R., Palmer, D. W., Patience, J., Perrin, M. D., Poyneer, L. A., Pueyo, L., Rajan, A., Rantakyr, F. T., Savransky, D., Schneider, A. C., Sivaramakrishnan, A., Soummer, R., Thomas, S., Wallace, J. K., Ward-Duong, K., Wiktorowicz, S. J., and Wolff, S. G., "DYNAMICAL MASS MEASUREMENT OF THE YOUNG SPECTROSCOPIC BINARY V343 NORMAE AaAb RESOLVED WITH THE GEMINI PLANET IMAGER," *The Astronomical Journal* **152**, 175 (Nov. 2016).

[30] Pegues, J., Czekala, I., Andrews, S. M., berg, K. I., Herczeg, G. J., Bergner, J. B., Ilsedore Cleeves, L., Guzmn, V. V., Huang, J., Long, F., Teague, R., and Wilner, D. J., "Dynamical Masses and Stellar Evolutionary Model Predictions of M Stars," *The Astrophysical Journal* **908**, 42 (Feb. 2021).

[31] Simon, M., Guilloteau, S., Beck, T. L., Chapillon, E., Folco, E. D., Dutrey, A., Feiden, G. A., Grosso, N., Pitu, V., Prato, L., and Schaefer, G. H., "Masses and Implications for Ages of Low-mass Pre-main-sequence Stars in Taurus and Ophiuchus," *The Astrophysical Journal* **884**, 42 (Oct. 2019).

[32] Mann, A. W., Dupuy, T., Kraus, A. L., Gaidos, E., Ansdell, M., Ireland, M., Rizzuto, A. C., Hung, C.-L., Dittmann, J., Factor, S., Feiden, G., Martinez, R. A., Ruz-Rodrguez, D., and Chia Thao, P., "How to Constrain Your M Dwarf. II. The MassLuminosityMetallicity Relation from 0.075 to 0.70 Solar Masses," *The Astrophysical Journal* **871**, 63 (Jan. 2019).

[33] Woillez, J., Abad, J. A., Abuter, R., Aller Carpentier, E., Alonso, J., Andolfato, L., Barriga, P., Berger, J.-P., Beuzit, J.-L., Bonnet, H., Bourdarot, G., Bourget, P., Brast, R., Caniguante, L., Cottalorda, E., Darr, P., Delabre, B., Delboulb, A., Delplancke-Strbele, F., Dembet, R., Donaldson, R., Dorn, R., Dupeyron, J., Dupuy, C., Egner, S., Eisenhauer, F., Fischer, G., Frank, C., Fuenteseca, E., Gitton, P., Gont, F., Guerlet, T., Guieu, S., Gutierrez, P., Haguenauer, P., Haimerl, A., Haubois, X., Heritier, C., Huber, S., Hubin, N., Jolley, P., Jocou, L., Kirchbauer, J.-P., Kolb, J., Kosmalski, J., Krempl, P., Le Bouquin, J.-B., Le Louarn, M., Lilley, P., Lopez, B., Magnard, Y., Mclay, S., Meilland, A., Meister, A., Merand, A., Moulin, T., Pasquini, L., Paufique, J., Percheron, I., Pettazzi, L., Pfuhl, O., Phan, D., Pirani, W., Quentin, J., Rakich, A., Ridings, R., Riedel, M., Reyes, J., Rochat, S., Santos Toms, G., Schmid, C., Schuhler, N., Shchekaturov, P., Seidel, M., Soenke, C., Stadler, E., Stephan, C., Surez, M., Todorovic, M., Valdes, G., Verinaud, C., Zins, G., and Ziga-Fernndez, S., "NAOMI: the adaptive optics system of the Auxiliary Telescopes of the VLTI," *Astronomy & Astrophysics* **629**, A41 (Sept. 2019).

[34] Cutri, R. e., Wright, E., Conrow, T., Fowler, J., Eisenhardt, P., Grillmair, C., Kirkpatrick, J., Masci, F., McCallon, H., Wheelock, S., et al., "Vizier online data catalog: Allwise data release (cutri+ 2013)," *VizieR Online Data Catalog* , II–328 (2021).

[35] Alibert, Y., Mordasini, C., Benz, W., and Winisdoerffer, C., "Models of giant planet formation with migration and disc evolution," *Astronomy & Astrophysics* **434**, 343–353 (Apr. 2005).

[36] Emsenhuber, A., Mordasini, C., Burn, R., Alibert, Y., Benz, W., and Asphaug, E., "The New Generation Planetary Population Synthesis (NGPPS). II. Planetary population of solar-like stars and overview of statistical results," *Astronomy & Astrophysics* **656**, A70 (Dec. 2021). arXiv: 2007.05562.

[37] Reffert, S., Bergmann, C., Quirrenbach, A., Trifonov, T., and Knstler, A., "Precise radial velocities of giant stars: VII. Occurrence rate of giant extrasolar planets as a function of mass and metallicity," *Astronomy & Astrophysics* **574**, A116 (Feb. 2015).

[38] Forgan, D., "Gravitational instability as a planet-forming mechanism," *42nd COSPAR Scientific Assembly* **42**, B1–3 (2018).

[39] Allard, F., Hauschildt, P. H., Alexander, D. R., Tamanai, A., and Schweitzer, A., "The Limiting Effects of Dust in Brown Dwarf Model Atmospheres," *The Astrophysical Journal* **556**, 357–372 (July 2001).

[40] Baraffe, I., Chabrier, G., Allard, F., and Hauschildt, P., "Evolutionary models for low mass stars and brown dwarfs at young ages," **211**, 41 (2003).